JOURNAL OF MATERIALS SCIENCE 33 (1998) 1421–1429

Laser-shock processing of aluminium-coated 55C1 steel in water-confinement regime, characterization and application to high-cycle fatigue behaviour

P. PEYRE, L. BERTHE, X. SCHERPEREEL, R. FABBRO
CLFA-LALP, Unité mixte ETCA-CNRS, 94114 Arcueil, France

55C1 steel was irradiated with a high-power neodymium–glass laser with application to induce plastic shock waves within targets, through the expansion of a laser-induced surface plasma. Laser-shock processing experiments were conduced in the plasma-confined regime with water to increase the laser-induced peak stresses. Physical, mechanical and processings aspects were reviewed, such as the characterization of stress waves in coated steels with a VISAR velocimeter system, and the mechanical changes induced in 55Cl in terms of compressive residual stresses or work-hardening levels. With the use of convenient protective coatings, some 7–8 GPa peak stress levels could be achieved which authorized the generation of high compressive residual stress levels (nearly 80% of the compressive yield strength), but preserved the surface integrity from detrimental roughening. Surface modifications performed under different shock conditions were shown to display some 30% increase on the bending fatigue limits of 55C1 at $R=0.1$. © *1998 Chapman & Hall*

1. Introduction

In the field of surface treatments, laser sources are usually used as flexible heat sources in investigation of solid-phase transformations [1], surface remelting (crankshaft applications) or surface alloying [2]. Among the wide variety of surface treatments investigated for improving properties of materials, laser-shock processing (LSP) was developed about 25 years ago in the USA [3, 4] with particular application to enhance fatigue properties of fastened joints for aeronautical applications. Many industrial materials were investigated at this time, such as aluminium or titanium alloys, or stainless steels, but because of the lack of reliable pulsed-laser sources (high cadency–high power density) and despite the satisfactory mechanical improvements displayed in aluminium- or titanium-based alloys, no real industrial application was shown to emerge. Since 1988, and with the support of automotive and aerospace partners, intensive work has been undertaken in France, including phenomenological and applied studies [5–9]. However, some critical processing questions still remain unanswered or need to be highlighted, such as

(i) the precise influence of absorptive coatings which can modify very strongly the stress loadings transmitted to the metal by type mismatch impedance effects,

(ii) the role played by laser-spot diameters on the stress-wave generation and propagation and on the resulting surface modifications,

(iii) the plastic flow limit characterization at very high strain rate and its influence on the residual stress generation.

All three processing aspects were reviewed with the objective to improve the fatigue life of steels which is one of the possible fields of application for LSP. This underlined the need to pay special attention to all the surface parameters influencing the fatigue behaviour, such as

(i) the compressive residual stress fields (X-ray diffraction) including stress amplitude levels, surface homogeneity aspects, and plastically affected depths,

(ii) the work-hardening levels with the use of X-ray peak broadening and Vickers hardness measurements,

(iii) the surface morphology modifications which are known to influence fatigue crack initiation.

In each case, experimental measurements were reported which allowed a state-of-the art to be drawn for LSP in a plasma-confined regime with water, and to evaluate its potential as a novel process to improve the properties of the near-surface region. On the other hand, the future potential of LSP was discussed, with attention focused on the emergence of new laser sources.

2. General trends in laser-shock processing of materials

Laser-shock processing (LSP) uses a high-energy (tenths of J) pulsed laser to irradiate a metallic surface

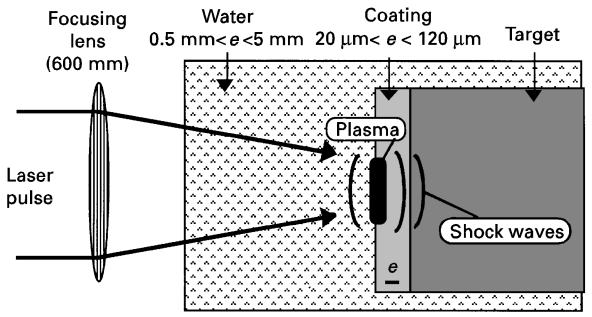

Figure 1 Laser-shock processing with a water-confinement regime.

during very short times (a few nanoseconds). When the laser pulse is focused on the surface to reach a GW cm^{-2} power density, it generates, through the expansion of a high-temperature (a few tens of thousands °C)–high-pressure (GPa range) surface plasma, a high-intensity shock wave which induces planar plastic strain in the metallic part. Conventional configuration, that was assessed in the 1968–1980 [3–5] period in the Battelle Columbus Institute (OH, USA) consists in covering the metal to be treated with a protective coating (to avoid thermal effects) and to immerse the area to be treated below a water overlay to improve the mechanical coupling by a confining-like effect (Fig. 1). Indeed, as the plasma is trapped between the target and the overlying water, its amplitude and duration are increased by factors of 10 (for the peak pressure level) and 3 (for the pulse duration) compared with direct ablation mode. Thus, the irradiated materials undergo no thermal process nor microstructural changes, except at very high pressures when pressure-induced phase transformations occur, such as $\gamma \rightarrow \alpha'$ on stainless steels (above 11–15 GPa) [7] or $\alpha \rightarrow \varepsilon$ on ferritic steels. Instead, the surface is submitted to uniaxial plastic strain, provided the stress-wave amplitude reaches a level superior to the shock yield strength of the target which is commonly termed the Hugoniot elastic limit (HEL).

All the investigations reported on LSP have been carried out with *Q*-switched neodymium–glass lasers operating at $\lambda = 1.06$ μm with 40–100 J output energies, 0.6–30 ns pulse durations and repetition rates ranging between 1 shot every 20–30 minutes (Battelle, USA, 1968–1980 [3–5] and 1 shot every 2–3 minutes (LALP, France, 1990–1996) [6, 9–11]. The power density range is usually in the 1–100 GW cm^{-2} range with pulses that are Gaussian in shape or exhibit short rise times [9]. Many processing aspects to be highlighted and optimized to ensure the best laser-material coupling as possible in terms of the plasma generation and most of all the stress-wave transmission to the substrate target. For instance, dielectric breakdowns occurring in the water have been shown to reduce the amount of energy reaching the surface at high power densities by creating a parasitic absorptive plasma at the water/air interface [11]. Above 10–15 GW cm^{-2}, the breakdown phenomenon limits the shock pressures to 5–6 GPa, shortens the pulse durations and, most of all, gives much more scattering to the peak-pressure values.

Of all the parameters influencing the transmission of a high-intensity stress wave to the substrate target at a given power density, the thermoabsorptive coating layer has been rarely investigated precisely, except by Fox [3]. In terms of compressive residual stress fields, all the previous studies have shown that LSP not only could have an affect much deeper than other surface processings (up to 2 mm depth), but also generated stress levels close to those generated by shot-peening [8,10].

In this paper we aim to draw, for the first time, correlations between the shock conditions stress loadings, …), the surface modifications and the mechanical behaviour of surface-treated samples after LSP.

3. Materials

Three different materials were used during our investigations; two of them (pure thin aluminium and AISI 316L stainless steel foils) were provided by Goodfellow SA, the last one was an industrial 55C1 medium carbon steel often used in automotive parts. Physical, acoustic and mechanical properties of the starting materials are shown in Table I, where ρ_0 is density, C_0 is bulk sound velocity, S is a material constant, Z is acoustic impedance is ρ_0, $D = \rho_0(C_0 + SU)$, σ_Y is tensile yield strength (quasi-static value), and E, ν are elastic constants (Young's modulus and anisotropy coefficient)

4. Characterization of laser-induced stress waves with the VISAR technique

4.1. The VISAR system for measuring back free velocities

The major contributor to the surface modifications generated by LSP is the stress pulse, $\Sigma = f(t)$ generated at the surface of materials by the plasma pressure while it represents the mechanical loading of the target (at the plasma–target interface we can write $P_{\text{plasma}} = \Sigma_{\text{target}}$). Many techniques have already been used to describe these mechanical impulses. Among these, piezoelectric quartz [9] or electromagnetic voltage (EMV) gauges [13] have provided very useful information, but limited by non-linear behaviour in

TABLE I Physical, acoustic (from [12]) and mechanical properties of the materials

Materials	ρ_0 (g cm^{-3})	C_0 (m s^{-1})	S	Z (g cm^{-2} s^{-1})	σ_Y (GPa)	E (GPa)	ν
Al-99.99% purity	2.7	5380	1.38	$1.45.10^6$	0.2	70	0.29
316L Stainless steel	7.9	4600	1.5	$3.7.10^6$	0.3	195	0.29
55C1 steel	7.8	4500	1.5	$3.6.10^6$	0.62	210	0.29

the case of quartz and by some magnetic field fluctuations in the case of EMV gauge. New piezoelectric copolymers also seem to be very promising but are still under investigation [14].

To understand and predict LSP effects on the metallic surface modifications, a precise characterization of laser-produced shock waves was conducted with a Doppler-laser velocimeter system called a velocity interferometer system for any reflector (VISAR). This technique interferometry is a newly developed [15] method for measuring free velocities induced by shock waves behind thin metallic targets. It has already been used to characterize the conventional shock loadings, but an original device has been developed in our laboratory by Tollier *et al.* [16] to identify the spallation thresholds in pure materials such as aluminium or copper (Fig. 2). Using an argon-probe laser focused (200 μm spot) at the back free surface of the targets, this system identifies the acceleration of interference f-ringes, which are dependent on the back free surface velocity, U_f, through a Doppler-like effect [15]. Assuming that shock and release parts of the Hugoniot curves are almost symmetrical (totally symmetrical when the stress level $\Sigma < 2$ HEL), this velocity, U_f, is approximately twice the particle velocity, U, behind the shock front ($U_f = 2U$) (Fig. 3). Lastly, by the use of the classical Rankine–Hugoniot conservation formula, one can access easily the stress-time loading profiles at the surface of the targets with

when $\Sigma <$ HEL

$$\Sigma = \rho_0 C_{e1} U$$

when $\Sigma >$ HEL

$$\Sigma = \rho_0 D U + 2/3\sigma_Y = \rho_0 (C_0 + SU)U + 2/3\sigma_Y \quad (1)$$

where Σ is the laser-induced peak stress, $2/3\sigma_Y$ is an elastic contributor corresponding to the deviatoric parts of the stress, ρ_0 the density, and C_{el} the longitudinal elastic velocity (6000 m s^{-1} on steels and 6500 m s^{-1} on aluminium alloys).

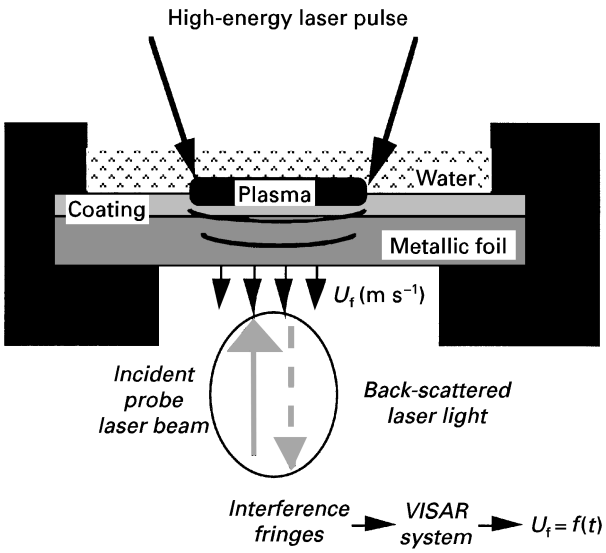

Figure 2 Schematic illustration of free velocity measurement with a VISAR system.

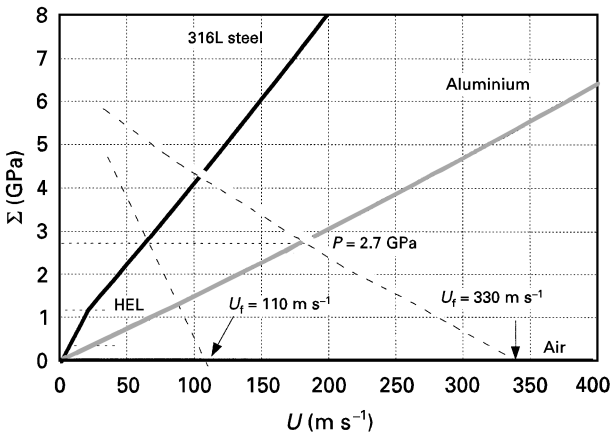

Figure 3 $\Sigma = f(U)$ curves for aluminium, steels and air (vacuum). Example of a 3–4 GW cm^{-2} LSP ($P = 2.7$ GPa): free velocity value = 330 m s^{-1} on aluminium alloys, = 110 m s^{-1} on 316L steel.

4.2. Shock-wave simulations

SHYLAC-1D hydrodynamic code [17] was used to simulate laser-induced free velocity profiles. This code is based on the method of finite differences and allows simulation of a laser energy deposit (J cm^{-2}) including the efficiency of the interaction, α, at the surface of the material in confined ablation mode. Coefficient α is known to be the energy ratio involved in the pressure rise, so $(1 - \alpha)$ E is devoted to the plasma formation [6]. During our simulations, this coefficient was estimated to 0.2–0.25, to give a good fitting with experimental measurements. This code includes a Mïe Gruneisen equation of state with reference to the Hugoniot curves of the materials (Fig. 3). A purely elastic–plastic behaviour was used for all the materials to evaluate the evolution of shock parameters (particle velocity, U, stress, internal energy, ...) in metallic targets.

4.3. Characterization of laser-induced loadings on aluminium-coated steels

During a laser-material interaction in the GW cm^{-2} range, the energy deposit and the ablation phenomenon occur on a few micrometres thus creating heat penetration to depths ranging between 10 and 20 μm. Consequently, during a conventional laser-shock, surfaces have to be protected by at least 20 μm thick coatings to provide only pure mechanical impulses to the targets. Irrespective of laser parameters (power density, pulse duration, pulse rise time, laser wavelength) which have been shown to influence the plasma pressure levels, the coating effects have to be estimated to precise laser-induced stress loadings submitted to materials.

Since the early works on LSP, many coatings have been used to ensure a thermal protection to metallic targets. These coatings can be metallic or organic paints or adhesives. The first atomic layers of the coating not only protect the surface from thermal rise but also from the plasma in itself, indicating that they can play a fundamental role on the plasma properties and particularly the plasma pressure. Most of all,

differences of acoustic properties, Z (Table I), at the interface between the surface coating and the underlying substrate can modify the stress loading by type mismatch impedance effects: if $Z_1 < Z_2$, the peak stress increases when the shock wave comes from material 1 to material 2. In this work, two of the usual protective coatings have been investigated: an aluminium-based paint with different thicknesses, and an aluminium-based adhesive of 100 μm (including 20 μm glue). Well-calibrated 200 μm 316L foils were used instead of 55C1 ones to draw general tendencies about LSP on aluminium-coated steels. At a given incident laser irradiance (about 4 GW cm^{-2} power densities), free velocity measurements were conducted on (i) bare 200 μm aluminium foils, (ii) bare 200 μm 316L stainless steel foils and (iii) 200 μm 316L + aluminium-based coatings at different thicknesses.

Figs 4–7 show the free velocity profiles as a function of time for each configuration. On aluminium foils impacted with 4 GW cm^{-2} (Fig. 4), the maximal free velocity amplitude is shown to be 320 ± 20 m s^{-1} (average value with at least three measurements) denoting an impact pressure $P = 2.8 \pm 0.2$ GPa (as shown by SHYLAC simulation and evidenced in Fig. 3). Pressure pulse duration at half maximum is close to 60 ns which is nearly twice the laser pulse duration. Reverberations of shock and release waves on the front and rear faces of the 200 μm foil give this oscillating aspect (successive velocity jumps) to the profile.

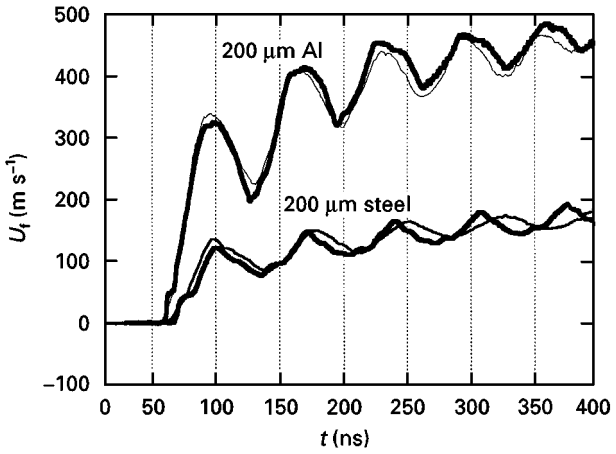

Figure 4 (——) VISAR velocity measurements at 3–4 GW cm^{-2} fluence on uncoated 316L and pure aluminium 200 μm foils. (——) SHYLAC-1D simulation (energy deposit = 20 J cm^{-2}).

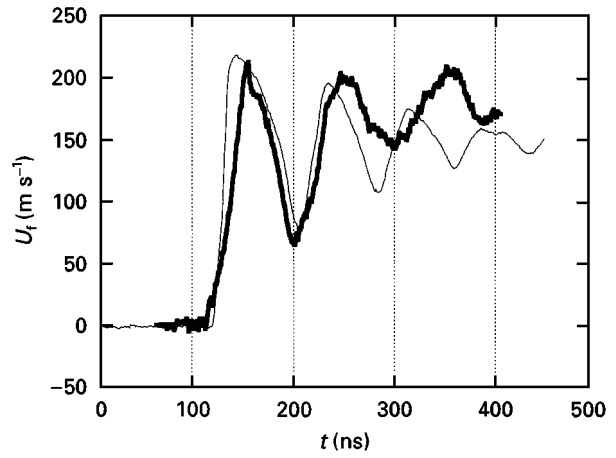

Figure 5 Back free velocity measurements at 3–4 GW cm^{-2} on 200 μm 316L foils coated with 130–140 μm aluminium paint ((——) VISAR measurement and (——) SHYLAC-1D simulation). The stress level increases from 2.7 GPa to 4.6 GPa on 316L with surface coating.

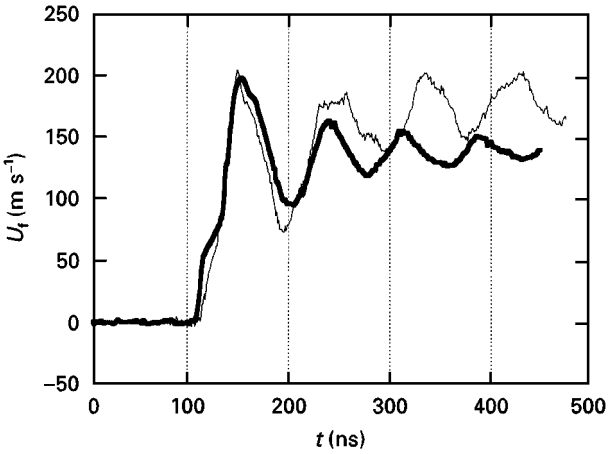

Figure 6 (——) VISAR measurement and (——) SHYLAC-1D simulation of LSP 3–4 GW cm^{-2} on 200 μm 316L coated with 100 μm aluminium adhesive.

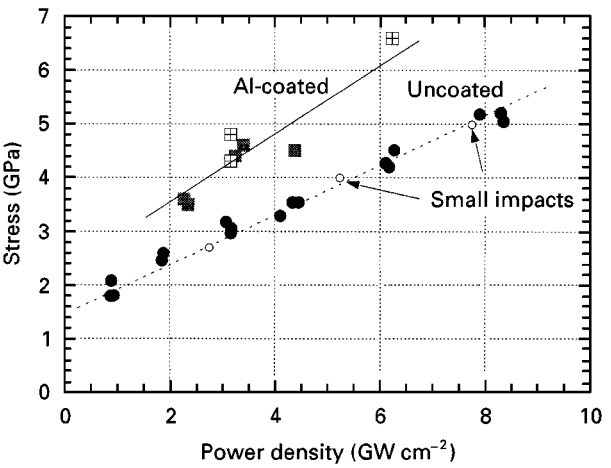

Figure 7 Stress $\Sigma = f$(power density) curve: influence of the coatings on the stress amplitude values. All measurements made with 3–4 mm impacts except three stress determinations made with 1 mm diameter spots. (○, ●) Base materials (aluminium or steels), (■) 316L + 140 μm aluminium paint, (■) 316L + aluminium adhesive.

On AISI 316L stainless steel, impedance mismatch effects occur and modify the profiles very strongly, as shown by a comparison between profiles of uncoated and coated steels (Figs 4–6). The free velocity amplitude is nearly 120 m s^{-1} on the bare steels, whereas it reaches 200–220 m s^{-1} with 140 μm coatings by impedance mismatch-like effects. In terms of stress levels, Σ, submitted to the metal, it increases from nearly the same level indicated on aluminium foils (2.7 ± 0.5 GPa) up to 4.5 ± 0.5 GPa. This very huge increase (+50%) happens with a shortening of the first velocity jump. In Fig. 6, the coating effects are also shown very clearly: for a lower coating thickness (90 μm Al + 10 μm glue versus 140 μm Al paint), the adhesive configuration displays almost the same velocity levels

(close to 220 m s^{-1} = 4.7 GPa). This was ascribed to the acoustic properties of glue which tend to increase the stress amplitudes. The stress levels deduced (with Equation 1) from several velocity measurements on coated steels at different power densities, are reported in Fig. 7 and compared with measurements on bare materials. From this stress $\Sigma = f$(power density) curve, we can conclude that coatings effects can play a very significant role in the case where their acoustic properties differ from those of the substrate (aluminium-base coatings on steels).

On steels, the large stress increases generated by aluminium-based coatings will have to be taken into account to optimize the shock conditions for materials hardening.

4.4. Laser spot-size effects

Recent investigations have shown that with a small impact configuration (0.5–1 mm), plastically affected depths could be strongly reduced by two-dimensional effects (Fig. 11 below). Our objective was also to confirm that surface stress levels were unmodified when reducing the impact sizes. We have reported in Fig. 7, pressure measurements performed with 1 mm impacts, where it is obvious that no detectable change has occurred with 1 mm instead of 4 or 5 mm impacts.

4.5. Determination of elastic–plastic transition during a laser-shock loading

LSP can be described as a planar compressive stress wave creating plastic strain in materials, provided the stress amplitude exceeds the shock yield strength under uniaxial loading (termed the Hugoniot limit HEL) of the base material. To optimize processing conditions, one must not only access the maximal stress level at the surface of the target, but also HEL values which depend on mechanical properties according to [18]:

$$\mathrm{HEL} = (1 - \nu)/(1 - 2\nu)\sigma_y^{dyn} \qquad (2)$$

where ν is the anisotropy coefficient and σ_y^{dyn} the compressive yield strength at high strain rate. In elastic–plastic solids, the stress waves transmitted through the specimen separate into two distinct waves: a leading elastic wave of HEL amplitude, and a plastic wave. The only means of determining HEL values is to analyse the amplitude of the elastic precursors of shock-wave profiles. These precursors are generally constant in depth, except on steels where attenuations have been shown to occur by many authors [19] on conventional shock loadings. The aim of this third part was to determine HEL values on all the materials investigated and to compare them with static values. Two examples of precursor determination are shown in Fig. 8 on 55C1 and 316L steels indicating that the free velocity values at the elastic–plastic inflection are close to 105 m s^{-1} on 55C1 steel and 50 m s^{-1} on 316L. With the use of Equation 1 below HEL (HEL = $\rho_0 C_{el} U_{HEL}$), this leads us to HEL values of 1.2 GPa on 316L and 2.5 GPa on 55C1. When a comparison is made with static σ_Y, HEL values give interesting information on the strain-rate dependence of the alloys. Indeed, as HEL = $(1 - \nu)/(1 - 2\nu)\sigma_y^{dyn} = 1.75\sigma_y^{dyn}$, one can easily deduce σ_y^{dyn} from the precursor values with σ_y^{dyn} = HEL/1.75. Consequently, at 10^6 s^{-1}, we have

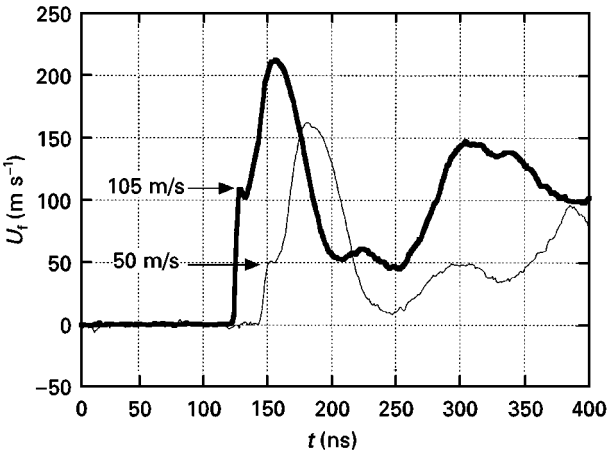

Figure 8 VISAR: elastic precursor determination on steels at 5 GW cm^{-2} and (——) 500 μm 316L or (——) 360 μm 55C1 coated with 90 μm aluminium paint (estimated surface stress = 6 GPa).

(i) on 316L

$$U_{f_{HEL}} = 50\ \mathrm{m\,s^{-1}}: \mathrm{HEL} = 1.2\ \mathrm{GPa},$$
$$\sigma_y^{dyn} = 0.7\ \mathrm{GPa} = 2.3\sigma_y$$

(ii) on 55C1

$$U_{f_{HEL}} = 105\ \mathrm{m\,s^{-1}}: \mathrm{HEL} = 2.5\ \mathrm{GPa},$$
$$\sigma_y^{dyn} = 1.4\ \mathrm{GPa} = 2.3\sigma_y$$

So it seems that both ferritic and austenitic steels are strain-rate dependent in the 10^{-3} s^{-1} (quasi-static) to 10^6 s^{-1} range. Indeed, more than a factor 2 was found between yield strengths values measured at 10^{-3} s^{-1}(σ_y) and estimated at 10^6 s^{-1}(σ_y^{dyn}) with elastic precursors. Moreover, as precursors tend to decrease in depth on steels [19], the HEL values are certainly underestimated by our VISAR estimations.

Lastly, on 55Cl steel, a decrease behind the precursor was noticed (Fig. 8). This phenomenon, already mentioned by many authors on steels [18] seems to be due to twin formations at the elastic–plastic transition.

4.6. Conclusion

In this section, we have described laser-induced shock waves in a water-confining regime with the use of a Doppler velocimeter system and with particular attention paid to the influence of the thermal absorptive coatings on the stress profiles. It has been shown on aluminium-coated steels that, with thick enough coatings (more than 50 μm), stress levels could be increased to a large scale, reaching +50%, as compared with stress levels obtained on bare materials. Moreover, confirmation was obtained that, even if small impacts can have detrimental effects on the shock-wave attenuation in depth, their surface stress

level is kept constant when compared to larger impacts.

Lastly, the elastic–plastic transition during shock loading was investigated and it was shown that steels are much more strain-rate dependent than aluminium alloys.

5. Surface modifications induced by laser-shock processing on 55C1 steel

5.1. Residual stresses

Residual stresses (RS) are usually known to be the key to enhanced mechanical properties such as fatigue or wear resistance. Consequently, most of our investigations have concentrated on determining surface and in-depth residual stresses induced by different shock configurations on different materials. In the case of LSP, they appear to be the result of a two-step mechanism: (1) a uniaxial compression during the laser-pulse generating tensile stretching of the surface layers, and (2) an opposite reaction of the surrounding zones (besides and below) which induces the compressive stress field. A recent calculation by Ballard *et al.* [8] has shown (Equations 2 and 3) that the laser-induced plastic deformation, ε^p (and therefore, the surface stresses, σ_{surf}), are linearly dependent on the (Σ:HEL) ratio. In fact, this ratio seems to be the most important parameter to optimize, but it necessitates a precise knowledge of Σ and HEL (as was done in Section 4). Indeed, according to Ballard *et al.* [8], and considering the case of a solid inclusion in a semi-infinite body with work-hardening effects taken as negligible, the maximum plastic deformations are achieved when $2HEL < \Sigma < 2.5HEL$. Plastically affected depths 'L' and maximum surface stresses, σ_{surf}, are then calculated from [8]

$$L = \frac{\Sigma}{2\mathrm{HEL}}\left(\frac{C_{el}C_{p1}\tau}{C_{el} - C_{p1}}\right) \quad (2)$$

$$\sigma_{surf} = \sigma_Y\left[1 - \frac{4\sqrt{2}}{\pi}(1+\nu)\frac{L}{r}\sqrt{2}\right] \quad (3)$$

where L is the plastically affected depth (mm), C_{el} and C_{p1} are elastic and plastic velocities (6000 and 4500 m s^{-1}, respectively, on steels), τ is the pressure pulse duration (nearly 50–60 ns for a 20–25 ns laser pulse), σ_{surf} the residual surface stresses (MPa), and r the radius of the impact (mm).

The X-ray diffraction technique by the $\sin^2\psi$ method was used to determine the residual surface stresses (RSS) induced by LSP. α-Fe (2 1 1) diffraction profiles were measured at 10 ψ angles and only 1 ϕ direction with CrK_α radiation at $2\theta = 156^\circ$ angle. Peak broadenings were evaluated using full-width at half-maximum (FWHM) after removal of the $K_{\alpha 2}$ radiation. Indepth stresses were obtained after step-by-step electropolishing of the impacted areas.

The two coating configurations previously investigated with VISAR were also used for the treatment of notched fatigue samples at the same power density (Fig. 9). With the aluminium paint configuration, two impact diameters were also used to estimate the spot-size effects. Residual stress measurements performed

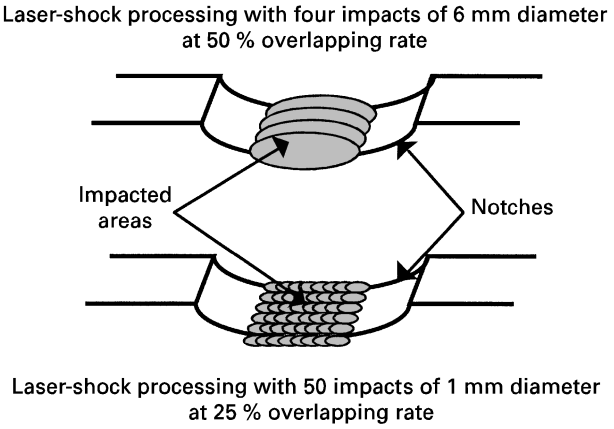

Figure 9 Laser-shock processing fatigue of notched samples with large or small impacts.

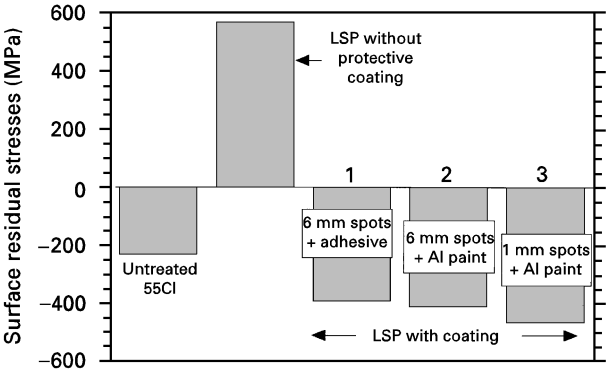

Figure 10 Average residual stress values determined at the surface of notched fatigue samples with different LSP conditions at 5 GW cm^{-2} in the water-confining regime: (**1**) 6 mm impacts + aluminium adhesive, (**2**) 6 mm impacts + aluminium paint, (**3**) 1 mm impacts + aluminium paint.

down the notch roots (Fig. 10) show that uncoated materials have very high tensile stress values even when confined with water. This was attributed to severe surface melting and confirms the overall influence of coatings to preserve the surface integrity. Among the three classical (protective coating + confining water) configurations, that for small impacts displayed the highest stress level (up to -460 MPa compared to -410 MPa with largest impacts and -390 MPa with aluminium adhesive). These stress levels are close to $-0.75\sigma_y$ which is roughly the maximal ratio previously achieved on aluminium alloys [10] or chromium–molybdenum steels [8]. On the other hand, the large impact configuration was shown to affect the metal at much greater depth than the small impact one as shown by measurements on plane samples exhibited in Fig. 11. This is due to two-dimensional attenuation of shock waves in the case of small impacts that reduce the plastically affected depths (800 μm for 1 mm impacts and 1200 μm for 6 mm impacts). It was also shown that LSP did not create any detectable X-ray peak broadenings after LSP (Fig. 12), except on uncoated materials where structural modifications during melting and solidification were shown to harden the superficial layers, thus increasing the FWHM values (from 1.4 to

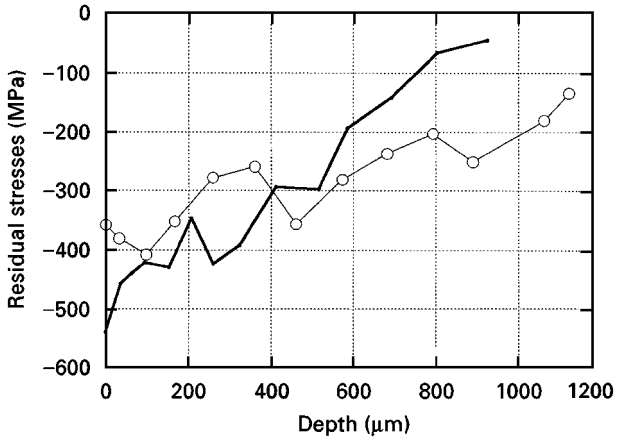

Figure 11 In-depth residual stresses on 55C1-LSP 5 GW cm^{-2}. Influence of impact sizes on the affected depths: (——) 1 mm, (○) 6 mm impacts.

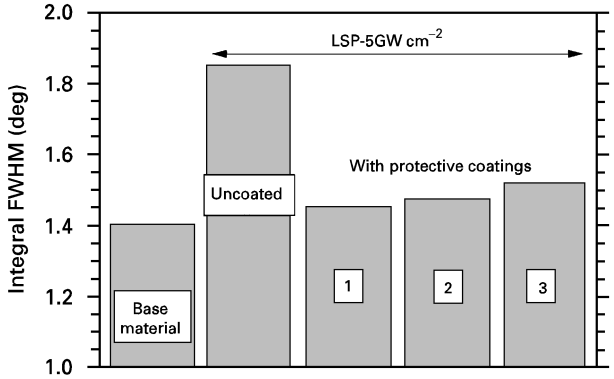

Figure 12 LSP effects on X-ray diffraction peak broadening (integral FWHM values).

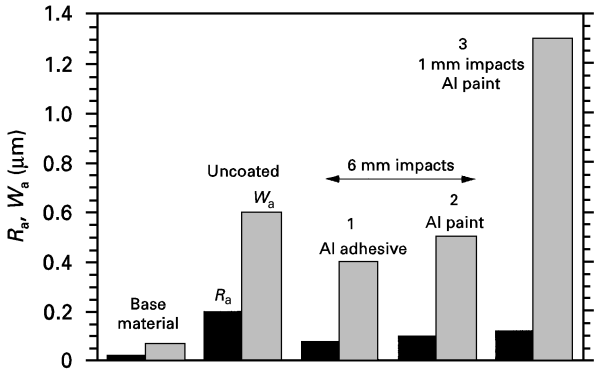

Figure 13 Surface morphology modifications as a function of LSP conditions (4–5 GW cm^{-2}).

1.85 = + 30%). This indicates that LSP generates low work-hardening levels and low densities of structural defects (dislocations, etc.) in 55C1.

5.2. Surface morphology modifications

Roughness and waviness measurements were made in order to analyse the surface geometry changes as a function of processing parameters. It is shown in Fig. 13 that LSP in the water-confinement regime + coating (configurations 1, 2, 3) keeps the surface roughness, R_a, globally unchanged (except for small impacts where a small roughening occurs from

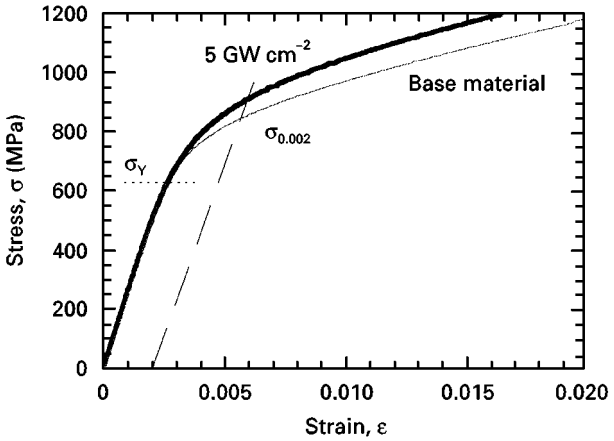

Figure 14 Stress–strain laws of 55C1 steel before and after LSP-5 GW cm^{-2} (extensometric measurements).

0.03–0.1 μm). However, surface undulations appear because of the ring-like pattern on the incident laser beam, and also because of overlapping regions. This phenomenon is clearly discernible in the case of small impacts where the average waviness parameter, W_a, increases from 0.07 μm to 1.25 μm (a factor of 20). The last point to notice is that uncoated material not only has tensile residual stresses but also has a deleterious surface state ($R_a = 0.2$ μm) because of surface melting.

6. Modifications of mechanical properties of 55C1 steel with LSP

6.1. Modifications of monotonic properties

Plane 55C1 samples were laser processed at 5 GW cm^{-2} to evaluate LSP effects on static properties. Extensometric strain-gauges were stuck to plane samples to estimate, during four-point monotonic bending, the effects of LSP in the water-confined mode on the $\sigma = f(\varepsilon)$ curve of the impacted surface (Fig. 14). After LSP, the 55C1 elastic–plastic behaviour is slightly modified, showing: no modifications of Young's modulus, E; no detectable change in σ_Y; a 10% increase in $\sigma_{0.002}$ (800 MPa to 890 MPa) due to an increase in the hardening modulus, h, of the surface layers in the first plastic strain steps.

However, because of the kinematic + isotropic hardening behaviour evidenced at the beginning of the plastic strain (curved aspect of the elastic–plastic transition), a quantitative evolution of h was difficult to calculate.

In conclusion, the laser-induced changes in plastic flow limits seems to be very low as compared with classical surface treatments like shot-peening or carbo-nitriding, which are known to create much higher increases in σ_Y but also a surface embrittlement [20].

6.2. Modifications of fatigue properties

Fatigue tests were carried out on notched specimen having a stress concentration factor $K_c = 1.65$ at $R = \sigma_{min}/\sigma_{max} = 0.1$ and a frequency $f = 30$ Hz with a four-point monotonic bending system. Fatigue limits, σ_D, were determined at 2×10^6 cycles. For the

TABLE II High-cycle fatigue results at $R = 0.1/f = 30$ Hz with a four-point bend test

σ_{max} (MPa)	Cycles to failure			
	Base material	1 mm impacts Al paint 4–6 GW cm^{-2}	7 mm impacts Al paint 5 GW cm^{-2}	7 mm impacts Al adhesive 5 GW cm^{-2}
350	2 NF at 2×10^6	–	–	–
400	1.1×10^6	–	–	–
	2 NF at 2×10^6			
450	5.89×10^5	–	2 NF at 2×10^6	2 NF at 2×10^6
	5.06×10^5			
500	4.01×10^5	2 NF at 2×10^6	$1.2 \times 10^6/6.2 \times 10^5$	$8.44 \times 10^5/6.76 \times 10^5$
	2.88×10^5	4.91×10^5	$^{**}2.1 \times 10^5$	$2.87 \times 10^5/^{*}2.2 \times 10^5$
550	2.48×10^5	NF-2×10^6	3.42×10^5	2.47×10^5
	2.69×10^5	$2.57 \times 10^5/^{**}2.16 \times 10^5$	3.58×10^5	
600	1.19×10^5	$1.41 \times 10^5/1.32 \times 10^5$	–	–

NF = non-failure at 2×10^6 cycles, *thermal effects, **crack initiation on the notch-edge

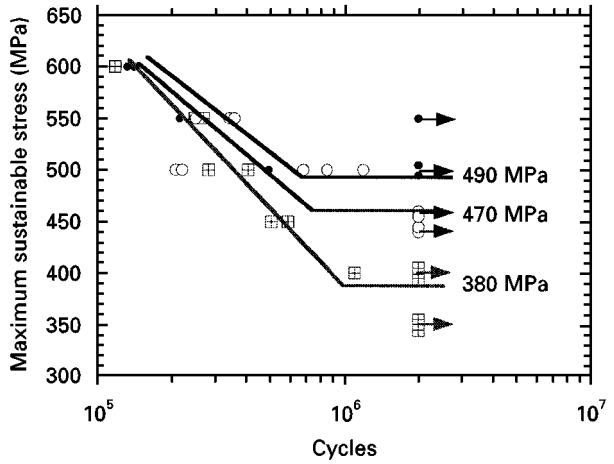

Figure 15 *S–N* curves of 55C1 – notched samples; bending test at $R = 0.1$. Effects of laser-shock processing with small or large impacts at 5 GW cm^{-2} in the water-confined mode. (●) 1 mm impacts, (■) base material; (○) 7 mm impacts.

determination of the Wöhler curve of the base 55C1, 12 samples were used. Among the 14 samples laser-processed with 7 mm impacts, 7 specimens were coated with 100 μm aluminium adhesive, the other 7 were coated with 100 μm aluminium paint. Lastly, 8 samples were treated with 1 mm impacts and 100 μm aluminium paint. Six applied stress levels were used, ranging between 350 and 600 MPa. All the results are shown in Table II. The same power densities (nearly 5 GW cm^{-2}) were used for each LSP configuration. As shown in Fig. 7, they resulted in stress levels close to 5 ± 0.5 GPa on the surface of 55C1 (nearly 2HEL). No detectable difference could be found between the two large impacts configurations which displayed roughly the same fatigue limit enhancements as compared with the base material (from 380 MPa to 470 MPa maximum sustainable stress). So a global *S–N* curve was drawn for the large impact configuration(Fig. 15). On the other hand, the small impact configuration displayed a somewhat better improvement with a 490 MPa fatigue limit at 2×10^6 cycles (+30%). These improvements also could be easily correlated to the differences in RS levels between the different configurations (see Fig. 10). Indeed, for a simple uniaxial bending test on notched samples, and assuming that RS is not subject to cyclic relaxation at $R = 0.1$, fatigue limits of surface-treated samples can be estimated from

$$\sigma_D(\text{after surface treatment}) = \sigma_D(\text{base material}) + \frac{|\Delta\sigma_{res}|}{Kt} \quad (4)$$

Using the RS average values shown in Fig. 10, one can easily deduce the fatigue limits of laser-shock processed samples ($\sigma_D = 470$ MPa $= 380 + (400 - 240)/1.65$ for the large impacts configuration and $\sigma_D = 490$ MPa $= 380 + (460 - 240)/1.65$ for the small impacts configuration). This subsequently confirms that no detectable stress relaxation has occurred in the shocked samples.

SEM investigations were also conduced on laser-shocked samples. It is found that part of the dispersion observed in the fatigue results could be attributed to machining defects leading to anticipated failures on the notch edges and not to the laser process itself. Only in one test (LSP with aluminium adhesive at 500 MPa), was the fatigue crack initiated on a thermally affected zone, thus indicating that LSP is globally a reliable process.

In conclusion, LSP could display a 30% maximal fatigue limit improvement on 55C1 steel with smaller impacts (1 mm) than that conventionally used (5–10 mm range). This improvement indicates that laser-shock processing with small impacts must be considered a good method for improving the fatigue life of structures. This is particularly important in considering future industrial applications of LSP where new excimer laser sources [21] will be able to deliver higher cadency rates (5–10 Hz) than have been previously used for LSP (0.1 Hz) but on smaller laser spot sizes (1–2 mm range) because of the smaller output energies (< 10 J).

7. Current trends in processing aspects

Many processing aspects need to be controlled during the experiments to ensure a good reproducibility and an industrial configuration to LSP. An original device

is used in LALP for materials processing. Of all the processing parameters requiring control, one should mention:

(i) the displacement of samples with a X–Y table;

(ii) a flowing water system to avoid water stagnancy with ablation dusts where parasitic breakdown effects are much more effective;

(iii) a photodiode + oscilloscope device to control the laser-pulse duration and energy;

(iv) an air-blast system with nozzles to protect the optical systems from water drops;

(v) a visualization of the areas to be treated;

(vi) a computer-controlled system to validate processing parameters and to command the X–Y displacement after each impact.

To date, this original system seems to be the most convenient for materials processing in an industrial configuration.

8. Conclusion

Laser-shock processing in the water-confinement mode was investigated at nearly 4–5 GW cm^{-2} power density range resulting, on uncoated materials, in pressure levels superior to 3 GPa. In the first part, using a laser Doppler velocimetry system (VISAR), we investigated the influence of thermoabsorptive coatings on the stress loadings submitted to the surface. It was confirmed that, by impedance mismatch effects, stress levels could be enhanced by more than 50%, thus allowing the treatment of harder materials than previously expected ($\sigma_Y > 2000$ MPa). It was also indicated that the coating thickness is an important contributor which has to be controlled and optimized to ensure a good mechanical coupling with the targets.

Therefore, plastic flow limits under laser-shock loading (HEL) were evaluated with the VISAR system and very high strain-rate dependences were shown for 55C1 and 316L steels, as compared with monotonic properties.

In the second part, surface modifications were investigated on 55C1 steel and particular distinctions were made between compressive residual stresses (RS) induced by small 1 mm impacts, as compared with conventional configurations (5–10 mm impact sizes). It was shown that overlapping 1 mm impacts could generate higher residual stress levels at nearly 5 GW cm^{-2} but with a somewhat higher roughness level. On the other hand, no real distinction could be made between residual stresses induced with the two different coatings investigated. However, the beneficial coating effects were confirmed because of tensile RS in evidence on uncoated 55C1.

Lastly, fatigue tests carried out on notched samples displayed about 30% maximum increases of the fatigue limits, σ_D, for a $R = 0.1$ bending test. The better improvements were displayed by the small impacts + aluminium-paint configuration, which seems to be rather promising for future applications of LSP involving a new generation of excimer lasers [20] delivering high-cadency rates but smaller impacts than conventional, because of smaller output energies.

Acknowledgement

The authors thank LM3 laboratory of the ENSAM-Paris for access to the X-ray diffraction equipments and for helpful cooperation during the experiments.

References

1. M. THEOBALT, P. MERRIEN and T. PUIG, in "Surface Modifications Technologies-SMTIII", edited by T. S. Sudarshan and D. G. Bhat (TMS, Warrendale, PA, 1990) p. 873.
2. B. L. MORDIKE, in: "Laser de puissance et traitements des matériaux", edited by A. B. Vannes (Presses Polytechniques et universitaires romandes; Lausanne, 1991) p. 176.
3. J. A. FOX, *Appl. Phys. Lett.* **24** (1974) 461.
4. A. H. CLAUER, B. P. FAIRAND and J. HOLBROOK, in: "Shock waves and high strain phenomena in metals", Vol. III edited by L. E. Murr (Plenum Press, New York, 1981) p. 675.
5. W. F. BATES, in "Proceedings of the ASM Conference on Applications of Lasers in Materials Processing" edited by A. E. Metzbower (ASM, Washington DC, 1979) p. 317.
6. R. FABBRO, J. FOURNIER, P. BALLARD, D. DEVAUX and J. VIRMONT, *J. Appl. Phys.* **68** (1990) 775.
7. M. HALLOUIN and M. GERLAND, *J. Phys IV* (*France*) **1** (1991) 519.
8. P. BALLARD, J. FOURNIER, R. FABBRO and J. FRELAT *ibid.* **1** (1991) 487.
9. D. DEVAUX, R. FABBRO, L. TOLLIER and E. BARTNICKI, *J. Appl. Phys.* **74** (1993) 2268.
10. P. PEYRE, R. FABBRO, P. MERRIEN and H. P. LIEURADE, *Mater. Sci. Engng* **A210** (1996) 102.
11. L. BERTHE, R. FABBRO, P. PEYRE, L. TOLLIER and E. BARTNICKI, In "Proceedings of the Europto-SPIE Conference on High Power Lasers: Applications and Emerging Applications" Besançon-France, June 1996, edited by Sayegh and Osborne p. 246.
12. D. J. STEINBERG, UCRL-MA-106439 report, February 1991.
13. P. PEYRE and R. FABBRO, *J. Phys. III* (*France*) **5** (1995) 1953.
14. M. BOUSTIE, S. COUTURIER, J. P. ROMAIN, D. ZAGOURI and H. SIMONNET, *Laser Particle Beams* **14** (2) (1996) 171.
15. L. M. BARKER and R. E. HOLLENBACH, *J. Appl. Phys.* **43** (1972) 4669.
16. L. TOLLIER, E. BARTNICKI and R. FABBRO, in "Proceedings of Europto-SPIE conference on High Power Lasers: Applications and Emerging Applications," Besançon-France, June 1996, edited by Sayegh and Osborne, p. 254.
17. J. P. ROMAIN and P. DARQUEY, *J. Appl. Phys.* **68** (1990) 1926.
18. J. N. JOHNSON and R. W. ROHDE, *J. Appl. Phys.* **42** (1971) 4171.
19. E. V. SHOROHOV, A. A. GORNOVOI and A. A. DENISENKO, *J. Phys IV* (*France*) **4** (1994) 409.
20. A. C. BATISTA, A. M. DIAS, P. VIRMOUX, G. INGLEBERT, T. HASSINE, J. C. LEFLOUR and J. L. LEBRUN, in "Proceeding of the 10th International Conference on Experimental Mechanics", edited by A. A. Balkema (Brookfield, Rotterdam, 1994) p. 739.
21. B. GODARD, M. STEHLE, P. MURER, J. BONNET and D. PIGACHE, *Opt. Soc. Am.* (*OSA*) *Tech. Digest Ser.* **11** (1993) 418.

Received 12 June
and accepted 5 December 1997